# Strong Amplified Spontaneous Emission from High Quality $GaAs_{1-x}Sb_x$ Single Quantum Well Nanowires

Xiaoming Yuan[a.b *], Dhruv Saxena[b], Philippe Caroff[b], Fan Wang[c], Mark Lockrey[d], Sudha Mokkapati[b], Hark Hoe Tan[b], Chennupati Jagadish[b]

a School of Physics and Electronics, Hunan Key Laboratory for Supermicrostructure and ultrafast Process, Central South University, 932 South Lushan Road, Changsha, Hunan 410083, P. R. China

b Department of Electronic Materials Engineering, Research School of Physics & Engineering, The Australian National University, Canberra, ACT 2601, Australia.

c Department of Physics and Astronomy, Faculty of Science, Macquarie University, Sydney, NSW 2109, Australia

d Australian National Fabrication Facility, The Australian National University, Canberra, ACT 2601, Australia.

*E-mail: xiaoming.yuan@csu.edu.cn

**Abstract**: Quantum confinement in semiconductor nanowires is of contemporary interest. Enhancing the quantum efficiency of quantum wells in nanowires and minimizing intrinsic absorption are necessary for reducing the threshold of nanowire lasers and is promising for wavelength tunable emitters and detectors. Here, we report on growth and optimization of $GaAs_{1-x}Sb_x/Al_{1-y}Ga_yAs$ quantum well heterostructures formed radially around a pure zinc blende GaAs core nanowires. The emitted photon energy from $GaAs_{0.89}Sb_{0.11}$ quantum well (1.371 eV) is smaller than the GaAs core, thus showing advantages over $GaAs/Al_{1-y}Ga_yAs$ quantum well nanowires in photon emission. The high optical quality quantum well (internal quantum efficiency reaches as high as 90%) is carefully positioned so that the quantum well coincides with the maximum of the transverse electric (TE01) mode intensity profile. The obtained superior optical performance combined with the supported Fabry-Perot (F-P) cavity in the nanowire leads to the strong amplified spontaneous emission (ASE). Detailed studies of the amplified cavity mode are carried out by spatial-spectral photoluminescence (PL) imaging, where emission from nanowire is resolved both spatially and spectrally. Resonant emission is generated at nanowire ends and is polarized perpendicular to the nanowire, in agreement with the simulated polarization characteristics of the TE01 mode in the nanowire. The observation of strong ASE for single QW nanowire at room temperature shows the potential application of $GaAs_{1-x}Sb_x$ QW nanowires as low threshold infrared nanowire lasers.

## 1. Introduction

III-V semiconductor nanowires have proven their potential as nanoscale optoelectronic and photonic devices with high performance thanks to their unique advantages, such as superior optical and electrical qualities,[1-7] flexibility in forming different types of heterojunctions and band alignments,[8-10] and ability to be integrated on Si substrates despite mismatch in the lattice-match constraints.[11, 12] In particular, they provide both a Fabry-Perot (F-P) microcavity and a gain medium for lasing to occur, and have been demonstrated in GaAs/$Al_{1-y}Ga_yAs$, GaSb, InP, InGaAs, GaN, ZnO, CdSe material systems.[4, 13-22] Moreover, efforts have been made to introduce quantum confinement in the nanowire to enhance its optical performance by incorporating quantum dot[23] and quantum wells (QWs)[24] in the nanowire or growing small diameter nanowires.[25] Radial QWs in nanowires confine electrons and holes in the radial direction and strongly increase the electron-hole wave function overlap. This architecture would be highly suitable for photonic and optoelectronic applications, such as light emitting diodes,[6, 26, 27] lasers,[24, 28] and ultra-fast photodetectors.[29] Thus, the growth of III-V QW nanowires has been extensively studied in the InGaAs/GaAs, GaAs/$Al_{1-y}Ga_yAs$, InGaAs/InP, InAs/InP, InAsP/InP, InGaN/GaN material systems.[24, 27, 30-33] Unfortunately, growing high quality and uniform QW around the nanowire remains extremely challenging due to the anisotropic crystal growth and composition inhomogeneity.[34, 35] As a consequence, lasing has only been demonstrated to date in InGaN/GaN and GaAs/$Al_{1-y}Ga_yAs$ QW nanowires.[24, 28, 36]

The radial GaAs/$Al_{1-y}Ga_yAs$ QW nanowire systems has been successfully developed thanks to the advantage of lattice matching between GaAs and $Al_{1-y}Ga_yA$ layers,[31] and applied for near infrared LEDs,[6] ultrafast photodetectors[29] and laser diodes.[28, 36] However, the emitted photons from the GaAs QW have a higher energy than that of the GaAs core, leading to a high threshold modal gain required for lasing due to intrinsic absorption in the cavity. Therefore, more QWs are required to enable lasing, which increases the complexity of growing these structures significantly. Instead, replacing GaAs QW with a lower bandgap semiconductor

could overcome this drawback since the core will not absorb the emitted radiation. Indeed, InGaAs/GaAs QW nanowires have been successfully grown and show good potential in optoelectronic applications.[9, 30] However, no attempts have been made on $GaAs_{1-x}Sb_x$ QW nanowires. In addition, the lateral growth behavior of $GaAs_{1-x}Sb_x$ has yet to be explored compared with their axial counterparts.

In this work, we study the growth and optical properties of $GaAs_{1-x}Sb_x/Al_{1-y}Ga_yAs$ QW structure grown on twin-free zinc-blende (ZB) GaAs nanowire cores. The growth behavior of $GaAs_{1-x}Sb_x$ QW is revealed in terms of faceting and compositional variations. The optimized QW nanowires show strong photoluminescence emission intensity, long carrier lifetime and high internal quantum efficiency at room temperature. In addition, cathodoluminescence (CL) spectra reveal uniform emission in the middle of the nanowire. Moreover, multiple peaks corresponding to the F-P cavity modes in the nanowire are observed in the PL spectra. Through spatial-spectral PL imaging, polarization dependent measurements and simulations, these amplified cavity modes are conclusively identified to be F-P cavity resonances of the TE01 guided mode. The observed high IQE and strong amplified PL emission from these QW nanowires demonstrate their promise for future low threshold infrared QW nanowire based lasers.

## 2. Methods

Nanowire growth was carried out in a horizontal flow metalorganic vapor phase epitaxy (MOVPE) reactor (Aixtron 200/4). The precursors used for Al, Ga, Sb and As were trimethylaluminum (TMAl), trimethylgallium (TMGa), trimethylantimony (TMSb) and arsine ($AsH_3$). The total gas flow was 15 l/min with ultra-pure $H_2$ as the carrier gas. First, taper-free GaAs nanowires were grown with 100 nm Au particles for 50 min using a standard two temperature process to guarantee its pure ZB phase.[37] Then, the growth temperature was raised

to 600~750 °C to favor lateral epitaxy via the vapor-solid growth mechanism. An $Al_{1-y}Ga_yAs$ shell with a nominal Al/(Al+Ga) ratio of 50% in the vapor phase was grown for 1.5 min before switching to $GaAs_{1-x}Sb_x$ QW and then the second $Al_{1-y}Ga_yAs$ barrier layer growth. The growth time for each layer was 3 min. Finally, a GaAs capping layer was grown for 5 min to protect the $Al_{1-y}Ga_yAs$ barrier from oxidation. All the radial layers were grown at the same temperature to avoid temperature induced compositional changes at the QW-barrier interfaces.[38] $Al_{1-y}Ga_yAs$ layer was grown under a total V/III ratio of 103 and TMGa flow of $0.734\times10^{-5}$ mol/min. TMGa flow rate, $AsH_3$/TMGa and TMSb/TMGa ratios for $GaAs_{1-x}Sb_x$ QW growth were $1.2\times10^{-5}$ mol/min, 1 and 0.75, respectively. The group III and V/III ratio used for GaAs capping layer were $1.62\times10^{-5}$ mol/min and 33, respectively.

After growth, nanowire morphology and crystal structure were examined by scanning electron microscopy (SEM, Zeiss Ultraplus) operated at 5 kV and transmission electron microscopy (TEM, JEOL 2100F) operated at 200 kV. The composition of the $GaAs_{1-x}Sb_x$ QW was determined by energy-dispersive X-ray (EDX) spectroscopy equipped in the TEM instrument. The detailed QW structure was revealed by high angle annular dark field scanning transmission electron microscopy (HAADF-STEM) studies of the cross sectional lamellae (30 nm thick) prepared by ultramicrotomy.[39]

The optical qualities of the QW nanowires were characterized by a home-built micro-photoluminescence (μ-PL) and time-resolved photoluminescence (TRPL) system.[40] Nanowires were transferred to a clean sapphire substrate mounted on the focus plane of the TRPL system. They were then excited by a pulsed laser with a wavelength of 522 nm, 300 fs pulse width and 20.8 MHz reputation rate, which is focused onto the sample through a 100× microscope objective lens (Nikon LU Plan, NA 0.9). At the laser repetition rate, 1 mW average laser power is equivalent to excitation pulse energy of 48 pJ. The spatial resolution of the system is limited by the spot size of the excitation laser, which is 0.3 μm for *x* (laser polarized direction) and

0.23 μm for *y* directions in the sample plane. With this spot size the average power density for 1 mW is $1.4 \times 10^9$ mW/cm$^2$. During power dependent PL experiments, 30 PL spectra were recorded with excitation power intensity over two orders of magnitude, from 0.039 to 3.337 μW. For TRPL, time correlated single photon counting (TCSPC) system was used with a system response of 45 ps.

For hybrid spatial-spectral mapping, an additional lens was inserted into the beam path to enlarge the laser beam to uniformly excite the nanowires. Nanowires were rotated and aligned parallel to the entrance slit of the spectrometer.[41] Thus, the spatial and spectral position can be distinguished in the hyperspectral image: the perpendicular direction (slit direction) represents the spatial position along the nanowire axis while the horizontal direction contains spectral information. For polarization-resolved PL experiments, a linear polarizer was inserted before the Si charge coupled device (CCD) detector with rotation accuracy of 0.3°. During the experiments, the polarizer was rotated 10° for each PL spectrum. The system response for polarization-dependent PL results was calibrated using a GaAs substrate which should be polarization independent. In addition to PL, cathodoluminescence (CL) technique was used to examine the luminescence uniformity of the QW nanowires. For this purpose, nanowires were dispersed onto a p+ Si substrate. CL spectra were collected at 2 kV using Peltier-cooled Si CCD array detector in a FEI Verios 460 system. Both PL and CL spectra were collected at room temperature.

## 3. Results and discussions

### 3.1 Growth of the $GaAs_{1-x}Sb_x$ QW nanowires: morphology, structure, polarity and composition

Figure 1a-b compares the typical morphology of the nanowire before and after $GaAs_{1-x}Sb_x$ QW growth. The (GaAs) nanowire cores present a non-tapered morphology with length around

7 μm. In contrast, subsequent radial growth alters the nanowire morphology. The QW nanowires show a large and irregular topmost segment, which plays an adverse effect for mode confinement. Its occurrence is probably caused by the surfactant role of Sb[42] and competition between vapor solid growth on the nanowire sidewall and vapor liquid solid growth through the Au nanoparticle.[43] Moreover, the bottom of the nanowires is slightly tapered due to faster lateral growth. The cross sectional HAADF-STEM image of a typical QW nanowire in Figure 1c-d shows the details of the QW structure. Here, the contrast is caused by atomic weight, leading to easier identification of different layers in the nanowire. GaAs and $GaAs_{1-x}Sb_x$ have larger atomic weight than the $Al_{1-y}Ga_yAs$ barrier, thus look brighter in the image, as illustrated by the schematic in the right hand side of Figure 1c. The whole cross section of the QW nanowire is a truncated hexagonal shape showing three-fold symmetry which is induced by polarity dependent crystal growth.[34] The upward direction can be conclusively determined to be [112]A according to the shape of the GaAs capping layer, since it grows faster in the [112]A orientation.[34] The QW thickness is measured along the [110] orientation. It decreases from ~7 nm (position A in Figure 1c) to ~2 nm (position B in Figure 1c). The average QW thickness is taken as 4.6 nm, measured from position C in Figure 1c. A closer inspection shows the formation of small {112}A facets after 3 min growth (see Figure 1d), indicating the slowest epitaxy rate along the [112]A direction for the QW. Indeed, in a sample where the QW growth time is increased to 16 min, the cross-sectional morphology of $GaAs_{1-x}Sb_x$ QW shows a truncated triangular shape with {112}A as the main facets (see Figure S1 in the Supporting Information). Here, the lateral growth of $GaAs_{1-x}Sb_x$ at high temperature presents a different growth behavior to that observed in $GaAs_{1-x}Sb_x$ nanowires,[42] showing {112}A instead of {110} side facets after long growth time. This result is in full agreement with a previous study of $GaAs_{1-x}Sb_x$/InP core/shell nanowire system which reports the surfactant role of Sb in favoring {112}A facets.[39]

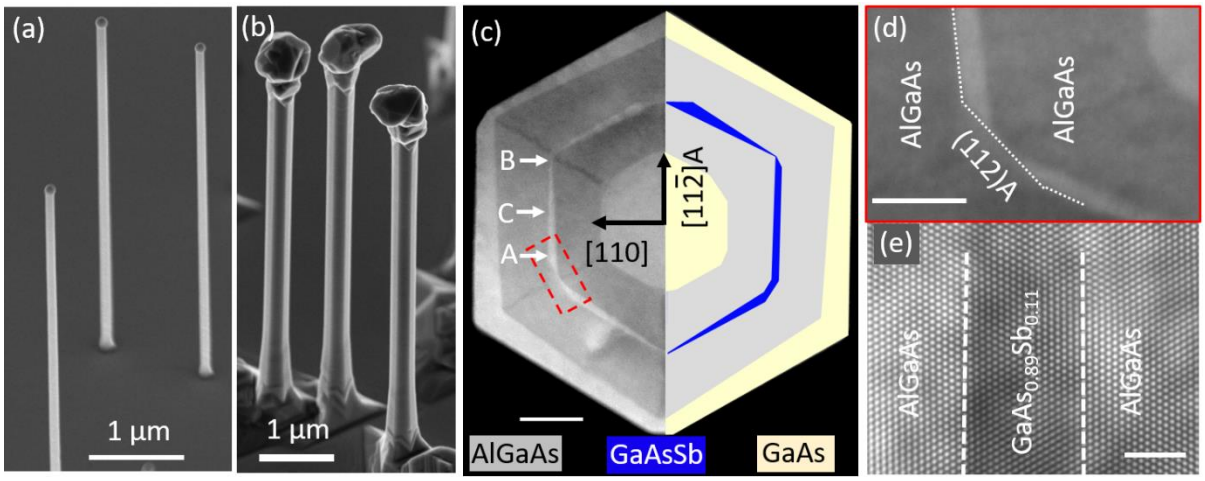


**Figure 1:** Morphology and structure of the $GaAs_{0.89}Sb_{0.11}$ QW nanowires grown at 725 °C. Scanning electron microscopy (SEM) images of (a) GaAs core nanowires and (b) $GaAs_{0.89}Sb_{0.11}$ QW nanowires. (c) Typical cross sectional HAADF-STEM image of the $GaAs_{0.89}Sb_{0.11}$ QW nanowires grown at 725 °C. The right hand side in (c) represents the schematic of the QW structure. The yellow regions represent GaAs, blue illustrates $GaAs_{0.89}Sb_{0.11}$ QW and the grey regions are the $Al_{1-y}Ga_yAs$ barriers. (d) Magnified HAADF-STEM image of the QW structure. (e) FFT of HRTEM at the QW region, showing the coherent interface. Scale bars are 50 nm in (c), 20 nm in (d) and 2 nm in (e).

Composition determination in the $Al_{1-y}Ga_yAs$ barrier layer and $GaAs_{1-x}Sb_x$ QW is carried out by EDX point analysis of a cross sectional sample where $GaAs_{1-x}Sb_x$ segment is grown for 16 min (see Figure S1). Sb and Al compositions in the $GaAs_{1-x}Sb_x$ segment and $Al_{1-y}Ga_yAs$ barrier are quantitatively determined by comparing the Ga/As element intensity ratio in the EDX spectrum with the standard spectrum taken from GaAs core (See the method and EDX spectrum in Figure S1b for more information). For QW nanowires grown at 725 °C, the Sb and Al contents are measured to be 11% and 52%, respectively. Assuming that the lattice constant of $Al_{1-y}Ga_yAs$ and $Ga_{1-x}As_xSb$ ternary compound satisfies Vegard's law, then the lattice constant of $GaAs_{0.89}Sb_{0.11}$ and $Al_{0.52}Ga_{0.48}As$ is 5.702 Å and 5.657 Å, respectively, leading to 0.8% lattice mismatch between the QW and the barrier. This level of strain does not cause any dislocations at the interface, as confirmed by the fast Fourier transform (FFT) filtered high

resolution transmission electron microscopy (HRTEM) image in Figure 1e. However it is worth mentioning that the moderate strain resulting from the lattice mismatch is still able to generate a few twin defects (twin density around 1~2 per micron) that propagate from the shell through the GaAs core (see Figure S2 in the Supporting Information).[44]

Growth temperature is found to play a major role in affecting the growth rate and composition of the QW. The QW thickness increases with growth temperature, from ~1.9 nm at 650 °C to 4.5 nm at 725 °C (See the structural information in Figure S3). In terms of composition, the precursor flow used for the $GaAs_{1-x}Sb_x$ growth should result in ~40% of Sb in the tapered $GaAs_{1-x}Sb_x$ nanowires grown at 500 °C.[42] However, the Sb content in the QW is only 11% at 725 °C. Easier decomposition of the $GaAs_{1-x}Sb_x$ compound and As-Sb exchange in $GaAs_{1-x}Sb_x$ QW at higher growth temperature can leads to lower Sb content in the QW.[45]

### 3.2 Optical properties of the QW nanowires: high IQE

The optical properties of the QW nanowires show a strong dependence on the growth temperature, as depicted in Figure 2a-b. For nanowires grown at lower growth temperature (625 °C), the PL emission intensity is quite low. In addition, PL emission from both GaAs core (871 nm) and the $GaAs_{1-x}Sb_x$ QW (~910 nm) could be observed in some nanowires. With increasing of growth temperature, GaAs core emission gradually disappears while only QW emission is observed and its signal intensity increases rapidly with growth temperature, indicating that radiative recombination occurs predominantly in the QW under high growth temperature (above 650 °C). The PL emission enhancement with growth temperature is ascribed to the material quality improvement of either the $Al_{1-y}Ga_yAs$ barrier or the $GaAs_{1-x}Sb_x$ QW. However, since $Al_{1-y}Ga_yAs$ barriers and $GaAs_{1-x}Sb_x$ QW were grown at the same temperature, it is difficult to clearly separate their individual contribution. It has been shown that the optimum temperature for $Al_{1-y}Ga_yAs$ layer is 750 °C.[46, 47] The strongest PL emission

intensity for the $GaAs_{1-x}Sb_x$ QW nanowires occurs at 725 °C. The PL spectrum shift with growth temperature does not show a clear trend, as both blue and red shifts are observed (see Figure 2a). Decrease of either the QW thickness or the Sb contents can lead to blue shift. According to the above structural analysis (see Figure S3), QW thickness increases with growth temperature while the Sb content drops. These two factors have opposite effects on the spectrum shift, thus leading to an unpredictable spectral shift.

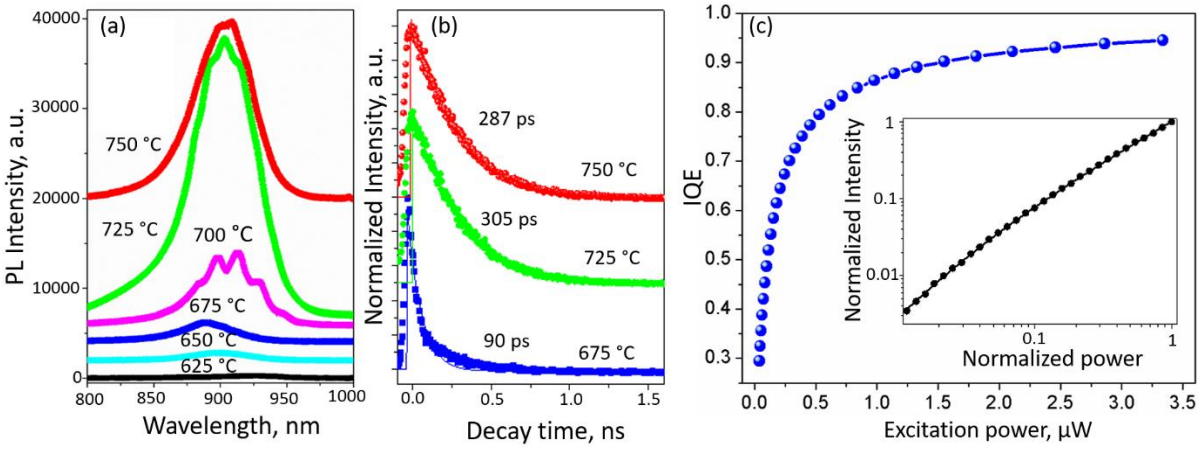


**Figure 2:** Comparison of (a) PL and (b) time-resolved PL spectra of QW nanowires grown at different temperatures. The spectra are shifted vertically for clarity. (c) Extracted internal quantum efficiency (IQE) of the QW nanowires grown at 725 °C from power dependent PL experiments. Inset shows fitted integrated PL intensity with excitation power.

Carrier lifetime measurements further confirm the effect of growth temperature on the optical quality of the QW nanowires, as shown in Figure 2b. When QW growth temperature is below 650 °C, the carrier lifetime is lower than the system resolution (~45 ps). Carrier lifetime is measurable (~90 ps) at 675 °C and quickly increases to 305 ps at 725 °C before dropping slightly to 287 ps at 750 °C. Native point defects exist during $GaAs_{1-x}Sb_x$ growth, leading to an unintentional p-type doping.[45, 48] However, these defects are not found to significantly weaken the luminescence intensity of QW nanowires. The long carrier lifetime together with strong luminescence of $GaAs_{1-x}Sb_x$ QW nanowires indicate excellent optical quality or high internal quantum efficiency (IQE). Applying our previous IQE determination method,[40] we did IQE analysis for single nanowire. In short, the emitted PL intensity can be expressed as:

$$I(P) \propto n_{rad} = \log\left(\frac{1}{n_0}\right) - \log\left(\frac{1+n_0}{n_0}\right) + n_0 \quad (1)$$

where $n_{rad}$ and $n_0$ represent carrier density involved in radiative recombination and initial carrier density generated by optical pumping which is proportional to the excitation power. By fitting the integrated PL intensity under different excitation power using equation (1), the IQE can be determined by IQE=$n_{rad}/n_0$. The power dependent PL spectra are shown in Figure S4. There is only a small blue shift of the QW emission wavelength during power dependent measurements of over two orders of magnitude due to the lifting of the Fermi level by photogenerated carriers. The power dependent integrated PL intensity fits well with the proposed model as shown in Figure 2c. IQE of nanowire increases rapidly with excitation power at low excitation power, reaching as high as ~80% at 0.5 μW. With excitation power beyond 1.5 μW, the measured IQE exceeds 90%. The high IQE and strong luminescence intensity demonstrate the excellent optical quality of the QW nanowires.

**3.3 Luminescence uniformity in the QW nanowires**

In nanowire growth, the emitted PL intensity and wavelength commonly varies along the length of the nanowire, particularly if they are ternary or quaternary materials.[35, 49, 50] Here we use CL to examine the luminescence uniformity of these QW nanowires since CL has higher spatial resolution than PL. The room temperature CL results for $GaAs_{1-x}Sb_x$ QW grown at 725 °C are shown in Figure 3. In general, CL emission intensity is strong, showing a single emission peak around 903 nm with FWHM of 54 nm (83 meV). The large FWHM is likely related to the thickness variation (see Figure 1c-d) and composition fluctuation in the QW. Emission peak from either GaAs core or $Al_{1-y}Ga_yAs$ barrier is not observed, indicating good confinement of the carriers in the QW. Qualitatively, the CL results correspond to the above PL results.

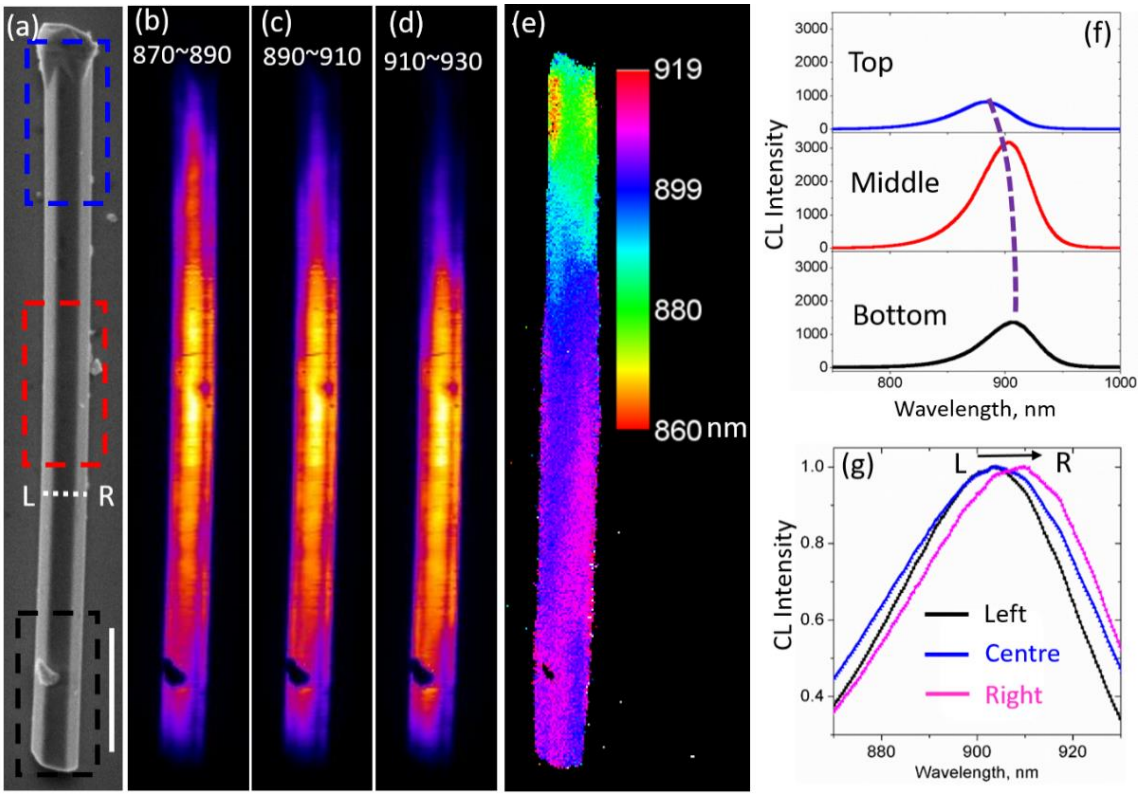


**Figure 3:** (a) SEM image of a QW nanowire dispersed on a Si substrate. (b-d) False color CL spectral mapping at various wavelength range: (b) 870~890 nm (c) 890~910 nm (d) 910~930 nm. (e) CL peak wavelength image. (f) CL spectra taken from the region indicated in (a), showing a spectra shift from bottom to top of the NW. The dotted line is a guide to the eye. (g) Three CL spectra taken across the NW (left, center and right hand sides of the nanowire). Scale bar in (a) is 1 μm.

Similar to the observed non-uniform luminescence intensity distribution in nanowires, [35, 49, 50] CL emission intensity of the $GaAs_{1-x}Sb_x$ QW nanowire is weaker at both ends of the nanowire (Figure 3a-e), especially at the nanowire top. This implies lower quality of the $GaAs_{1-x}Sb_x$ QW at bottom and top of nanowire, which is probably caused by local growth condition differences. Apart from that, emission intensity is uniform for the rest of nanowire. CL spectral mapping (Figure 3e) and the corresponding CL spectrum (see Figure 3f-g) reveals a slight spectral shift along the nanowire. Overall, the spectrum peaks at higher energy (1.404 eV (~883 nm) at nanowire top and gradually decreases to 1.371 eV (~904 nm) at the middle of nanowire and maintains fairly constant till the bottom end of nanowire. In particular, the emitted photon

energy differs slightly in the radial direction of the nanowire (Figure 3e). For instance, CL line scan across the QW nanowire reveals a spectral shift of 5 nm (Figure 3g). Several factors may contribute to this effect. First, Sb content distribution in the QW can vary along the nanowire and changes in different growth directions due to anisotropic crystal growth. In addition, the QW thickness is not uniform in the nanowire as revealed by the cross-sectional HAADF-STEM image in Figure 1. However, this spectral shift is very small compared with the large FWHM.

### 3.3.2 Amplified spontaneous emission and mode characterization

The high IQE, uniform luminescence distribution and F-P cavity formed by the nanowires leads to the observation of regularly-spaced multiple peaks in the spectrum for some nanowires (see Figure 2). Indeed, for the QW nanowires grown at the optimal temperature of 725 °C, strong resonant emission is observed even at room temperature, showing great potential for lasing. Figure 4a shows a spatial-spectral PL image of a QW nanowire grown at 725 °C. Through this image, the generation of amplified spontaneous emission (ASE) can be distinguished from the spontaneous emission (SE). Intense emission coming from the nanowire ends is observed at certain spectral positions, which confirms that ASE is due to F-P type resonant modes in the nanowire cavity. In contrast, SE is generated in the main body of the nanowire. In the hyperspectral image, each horizontal line represents a spectrum from different parts of the nanowire (along its axis). By integrating it, we obtain the total emission spectrum from different parts of the nanowire (the marked region in Figure 4a), as shown in Figure 4b. In the main body of the nanowire, PL emission mostly consists of SE with a broad emission peak around 840 nm (blue curve in Figure 4b), which is likely from the GaAs core. The peak is shifted to shorter wavelengths because the carrier density in the GaAs core is large due to strong optical pumping and carriers overflowing from the QW. At both nanowire ends, strong periodic emission peaks (ASE) are observed in the wavelength range from 810 to 940 nm, which is ascribed to the longitudinal modes of the F-P cavity formed in the nanowire. The

spacing between the peaks is between 13 to 15 nm. For F-P cavity in a nanowire, the mode spacing is determined by the following equation:[51]

$$\Delta\lambda = \lambda^2 / \{2L[n - \lambda(dn / d\lambda)]\} \quad (2)$$

where λ is the average wavelength between two periodic peaks, *L* is the nanowire length and the *n* is refractive index of $GaAs_{0.89}Sb_{0.11}$. The nanowire length transferred to the sapphire substrate is measured to be around 5.3 μm. In the wavelength range of 810-915 nm, the group index $n_g$ ($n - \lambda(dn / d\lambda)$) of $GaAs_{0.89}Sb_{0.11}$ QW nanowire is estimated to be in the range of 4.9-5.1.[52, 53] Thus the calculated mode spacing in the above wavelength range is from 12.8-15.7 nm, agreeing well with the measured values. In $GaAs_{1-x}Sb_x$ QW nanowires, the bandgap of GaAs is larger than the $GaAs_{1-x}Sb_x$ QW emission energy, thus the GaAs core is transparent to the QW emission. As a result, the nanowire serves as a low-loss cavity and is the reason for the observed ASE even at low excitation. In QW nanowires, the emission couples to different cavity modes and shows different types of polarization characteristics. The coupling depends on the placement of the QW in the nanowire and the polarization of light emission from the QWs. To identify the mode preference in the $GaAs_{1-x}Sb_x$/AlGaAs QW nanowires, numerical methods (Mode Solutions, Lumerical) are used to calculate the guided modes in the nanowire. The nanowire heterostructure is modelled using dimensions measured from cross-sectional HAADF-STEM images. The nanowire has a hexagonal cross-section and is lying on a sapphire substrate. GaAs core diameter is set as 100 nm. The inner and outer $Al_{1-y}Ga_yAs$ barrier is determined to be 33 and 38 nm, respectively. QW thickness variation is ignored during the modelling and an average value of 4.6 nm is used. The GaAs capping layer is 16 nm. Material parameters for GaAs, $GaAs_{0.89}Sb_{0.11}$ and sapphire are obtained from literature[54] and the mode free-space wavelength is 894 nm.

From simulations, two possible modes are supported, TE01 and $HE11_b$, as presented in Figure 4c-d. For TE01 mode, the mode intensity is mostly localized in the middle between the core and GaAs capping layer, strongly overlapping with the QW layer. $HE11_b$ mode is another possible cavity mode. The intensity of $HE11_b$ mode is mainly concentrated in the GaAs core and shows much less overlap with the QW gain medium. In addition, $HE11_b$ mode has lower reflectivity from end facets than TE01 mode (from simulations).[4] As a consequence, TE01 mode will be amplified more compared with $HE11_b$ mode. Thus, the ASE peaks observed in the measurements can be assigned as emission from the TE01 mode.

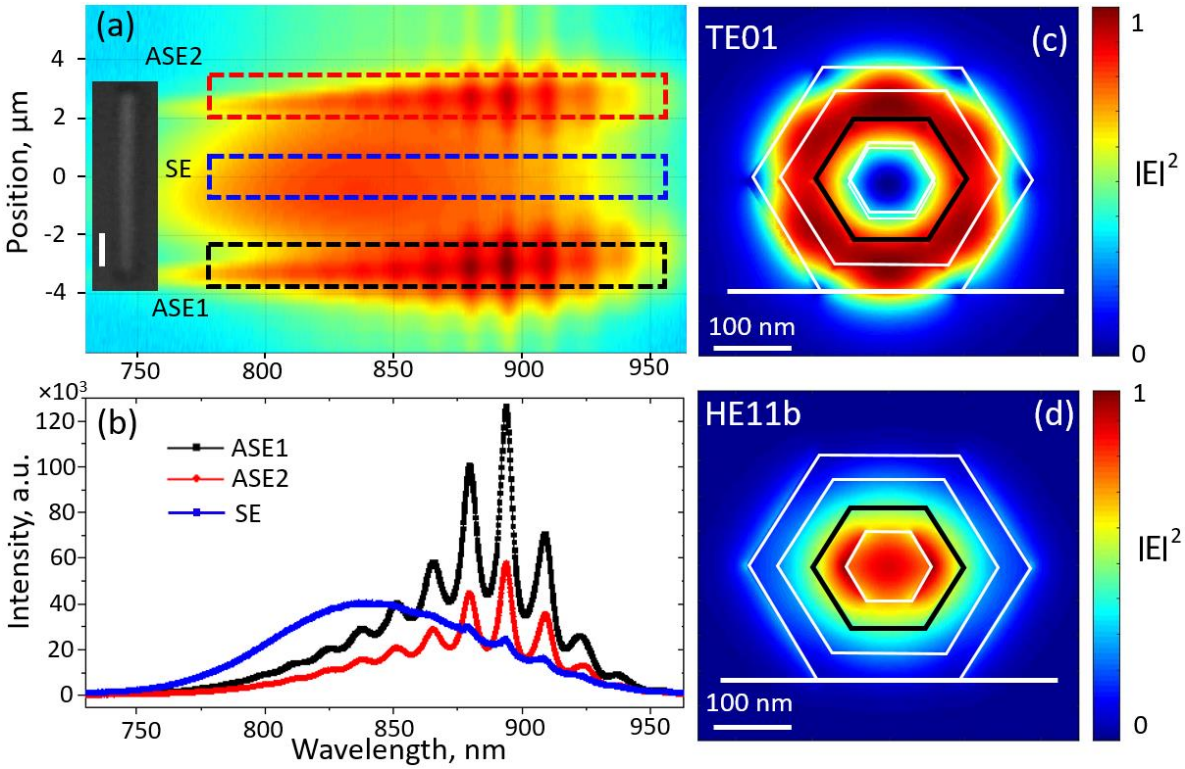


**Figure 4:** 1D hyperspectral map of one QW nanowire grown at 725 °C, showing strong ASE at the two ends of the nanowire. Inset illustrates the position of the nanowire (b) Corresponding emission spectra from three different regions of the nanowire as indicated in (a). (c-d) Simulated electric field intensity profile of TE01 mode and $HE11_b$ mods supported in the nanowire, respectively. The outline of the heterostructure is shown by the lines with thick dark line indicating the position of the QW. The scale bar for the optical image in (a) is 1 µm.

Since the polarization dependent intensity of the cavity mode shows different trends, it can be used to further clarify the supported mode in the nanowire. We performed finite-difference time-domain (FDTD) simulations using a commercially available software package (FDTD Solutions, Lumerical) to obtain the far-field profile of different guided modes. In these simulations, guided modes supported in the nanowire are injected along the nanowire axis and a monitor is placed above the nanowire to record the near-field mode profile.[55] The far-field mode profile is calculated from the near-field data using numerical methods. The components of the electric field parallel and perpendicular to the nanowire are then calculated from the far-field profiles. The mode polarization determined from the simulations is then compared with experimental results. During the simulation, the horizontal direction is parallel to the nanowire. The simulated polarization characteristics of three different modes in the nanowires are shown in Figure 5.

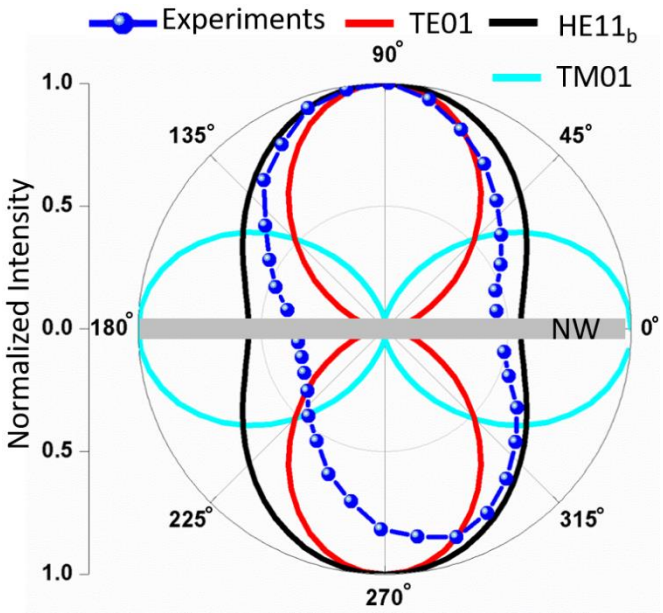


**Figure 5**: Polarization-dependent intensity of guided modes (TM01, TE01 and $HE11_b$) from simulations. The polarization dependence of ASE from the nanowire obtained from experimental measurements is also shown.

TM01 mode is polarized parallel to nanowire and is mostly valid for nanowire core emission.[56] TE01 and $HE11_b$ modes are both polarized perpendicular to the nanowire, showing difference only in the degree of linear polarization, which is defined as:

$$\rho = \frac{I_{//} - I_{\perp}}{I_{//} + I_{\perp}} \tag{3}$$

where $I_{//}(I_{\perp})$ is the emission intensity in the far field (or integrated spectral intensity) parallel/perpendicular to the nanowire. Based on the simulation results, TE01 mode has a smaller polarization ratio ( $\rho_{TE}$ = -0.95) than that of the $HE11_b$ mode ( $\rho_{HE}$ =-0.29). Polarization dependent PL intensity for ASE is determined by integrating the peak intensity at 894 nm (the strongest ASE peak) according to the hyperspectral image in Figure 4a-b. The obtained results are compared and plotted together with the simulated results in Figure 5. The measured ASE intensity is the strongest when perpendicular to the nanowire. Experimentally, the degree of linear polarization is determined to be -0.48. Experimentally determined intensity of ASE contains contribution from SE. SE is polarized parallel to nanowire, thus showing a positive value of $\rho_{SE}$. Therefore, the measured $\rho_{ASE}$ should be larger than the theoretical value. If it is $HE11_b$ mode, $\rho$ must be larger than -0.29, which disagrees with our experimental results. As a consequence, the observed ASE in the $GaAs_{1-x}Sb_x$ QW nanowires can thus be confirmed to be the TE01 mode. The experimental results show a slight discrepancy to the simulated TE01 mode, since the nanowire end facets are not that sharp as modelled in the simulation and the experimental results contain contribution from spontaneous emission.

Due to the strong overlap between the TE cavity mode and the QW gain region, ASE can be observed at room temperature at low excitation fluence. The occurrence of ASE suggests good optical cavity and high internal quantum efficiency of these QW nanowires, and is promising for lasing. It has been demonstrated in GaAs/AlGaAs QW nanowire lasers that the

cavity loss due to photon absorption in the GaAs core and capping layer is significant, resulting in large cavity loss (or threshold modal gain).[36] In our $GaAs_{1-x}Sb_x$ QW nanowire, absorption is avoided since the QW emitted photon energy is smaller than the band gap of bulk GaAs, so these nanowire cavities are predicted to have lower loss (or threshold modal gain) than GaAs/AlGaAs QW nanowire lasers. The mode quality factor (Q) is determined by fitting the PL spectrum with Lorentzian function (See Figure S5 for detailed information). Even though, the QW thickness variation reduces the material gain and thus is not favorable for obtaining nanowire lasing, the obtained highest mode Q factor in this work is 145 under excitation power density of 140 W/cm$^2$, which is much larger than those in the InGaAs/GaAs quantum nanowires measured at 80 K.[30] The threshold gain ($g_{th}$) required for lasing can be calculated by the following equation:[36]

$$g_{th} = \frac{2\pi}{\lambda} \cdot n_g / (Q \cdot \Gamma) \quad (4)$$

where $\lambda$ and $\Gamma$ represent lasing wavelength and mode confinement factor, respectively. Here $\lambda$ is chosen as 894 nm. $n_g$ and $\Gamma$ for $TE_{01}$ mode are estimated to be 5 and 0.05, respectively. The obtained $g_{th}$ is $4.8\times10^4$ cm$^{-1}$, which is ~9 times larger than $g_{th}$ in GaAs/AlGaAs multi-QW nanowire lasers.[36] Consequently, increasing the laser pumping power only results in saturation of ASE together with blue shift of the whole PL spectrum instead of lasing. The large $g_{th}$ is due to the small Q and $\Gamma$ in our nanowires. The threshold gain can be reduced by increasing the number of QWs (to increase the modal gain) and by increasing the length of the nanowire (to reduce the mirror loss). According to calculations, a minimum of 3 QWs are required for room-temperature lasing, provided that the MQWs have uniform thickness, are uncoupled and are placed such that the overlap between QW and $TE_{01}$ mode is maximum.[36] However, a large amount of work on growth optimization is required to achieve this goal, since the growth conditions for a multi-QW structure can be quite different to those of a single QW nanowire.

For instance, it has been demonstrated that the GaAs QW growth rate varies with nanowire diameter.[36]

## 4 Conclusions

In conclusion, high quality strained $GaAs_{0.89}Sb_{0.11}/Al_{1-y}Ga_yAs$ QW nanowires have been grown and optimized via MOVPE. Despite the strain induced twin formation in the QW nanowires, the interface between $GaAs_{0.89}Sb_{0.11}$ and the $Al_{1-y}Ga_yAs$ layer still remains coherent, resulting in high optical quality. The QW growth rate/thickness increases with growth temperature while the Sb content in the QW shows a decreasing trend, leading to complicated dependency of the PL spectrum shift with growth temperature. Moreover, there is a difference in polarity dependent crystal growth between GaAs and $GaAs_{1-x}Sb_x$. [112]B is the slowest growth direction for GaAs but the fastest for $GaAs_{1-x}Sb_x$. After sufficient growth time of $GaAs_{1-x}Sb_x$ QW, the side facets evolve gradually from {110} to mainly {112}A facets.

The optical quality of the $GaAs_{1-x}Sb_x$ QW nanowires improves significantly with growth temperature until 725 °C where a strong PL emission around 903 nm is observed at room temperature with carrier lifetime of 305 ps and high IQE at low excitation power. Luminescence is rather uniform along the nanowire with insignificant peak wavelength variation in the spectrum. Hybrid spatial-spectral mapping shows strong ASE at both ends of the nanowire in the wavelength range of 810~930 nm and uniform SE from the nanowire body. Resonant emission peaks are caused by the longitudinal mode of the F-P cavity. Resonant PL emissions are strongly polarized perpendicular to the nanowire. Simulation shows strong overlap between the TE01 mode and QW region. Polarization dependent PL and simulation results confirm that the periodic peaks are TE01 mode. These high quality $GaAs_{1-x}Sb_x$ QW nanowires are a promising candidate for low threshold QW nanowire lasers.

**Supporting Information Available:**

Crystal structure and optical properties of $GaAs_{0.89}Sb_{0.11}$ QW nanowires.

This material is free of charge via the Internet at http://pubs.acs.org/.

**Acknowledgements**

The Australian Research Council is acknowledged for financial support. Access to facilities used in this work is made possible through the Australian National Fabrication Facility, ACT Node and Australian Microscopy and Microanalysis Research Facility.

**References**

(1) Yang, Z.-x.; Yip, S.; Li, D.; Han, N.; Dong, G.; Liang, X.; Shu, L.; Hung, T. F.; Mo, X.; Ho, J. C. Approaching the Hole Mobility Limit of GaSb Nanowires. *ACS Nano* **2015,** *9,* 9268-9275.

(2) Önder, G.; David, J. v. W.; Ilse van, W.; Diana, C.; Sébastien, R. P.; Erik, P. A. M. B.; Leo, P. K. Towards high mobility InSb nanowire devices. *Nanotech.* **2015,** *26*, 215202-215208.

(3) Wallentin, J.; Anttu, N.; Asoli, D.; Huffman, M.; Åberg, I.; Magnusson, M. H.; Siefer, G.; Fuss-Kailuweit, P.; Dimroth, F.; Witzigmann, B.; et al. InP Nanowire Array Solar Cells Achieving 13.8% Efficiency by Exceeding the Ray Optics Limit. *Science* **2013,** *339,* 1057-1060.

(4) Saxena, D.; Mokkapati, S.; Parkinson, P.; Jiang, N.; Gao, Q.; Tan, H. H.; Jagadish, C. Optically pumped room-temperature GaAs nanowire lasers. *Nat. Photon.* **2013**, *7*, 963-968.

(5) Tomioka, K.; Fukui, T. Tunnel field-effect transistor using InAs nanowire/Si heterojunction. *Appl. Phys. Lett.* **2011,** *98*, 083114-083116.

(6) Tomioka, K.; Motohisa, J.; Hara, S.; Hiruma, K.; Fukui, T. GaAs/AlGaAs Core Multishell Nanowire-Based Light-Emitting Diodes on Si. *Nano Lett.* **2010**, *10*, 1639-1644.

(7) Dai, X.; Zhang, S.; Wang, Z.; Adamo, G.; Liu, H.; Huang, Y.; Couteau, C.; Soci, C. GaAs/AlGaAs nanowire photodetector. *Nano Lett.* **2014**, *14*, 2688-2693.

(8) Plissard, S. R.; van Weperen, I.; Car, D.; Verheijen, M. A.; Immink, G. W. G.; Kammhuber, J.; Cornelissen, L. J.; Szombati, D. B.; Geresdi, A.; Frolov, S. M.; et al. Formation and electronic properties of InSb nanocrosses. *Nat Nano.* **2013**, *8*, 859-864.

(9) Spirkoska, D.; Arbiol, J.; Gustafsson, A.; Conesa-Boj, S.; Glas, F.; Zardo, I.; Heigoldt, M.; Gass, M. H.; Bleloch, A. L.; Estrade, S.; et al. Structural and optical properties of high quality zinc-blende/wurtzite GaAs nanowire heterostructures. *Phys. Rev. B* **2009,** *80,* 245325-245333.

(10) Borg, B. M.; Dick, K. A.; Ganjipour, B.; Pistol, M. E.; Wernersson, L. E.; Thelander, C. InAs/GaSb Heterostructure Nanowires for Tunnel Field-Effect Transistors. *Nano Lett.* **2010**, *10*, 4080-4085.

(11) Munshi, A. M.; Dheeraj, D. L.; Fauske, V. T.; Kim, D. C.; Huh, J.; Reinertsen, J. F.; Ahtapodov, L.; Lee, K. D.; Heidari, B.; van Helvoort, A. T. J.; et al. Position-Controlled Uniform GaAs Nanowires on Silicon using Nanoimprint Lithography. *Nano Lett.* **2014**, *14*, 960-966.

(12) Conesa-Boj, S.; Kriegner, D.; Han, X.-L.; Plissard, S.; Wallart, X.; Stangl, J.; Fontcuberta i Morral, A.; Caroff, P. Gold-Free Ternary III–V Antimonide Nanowire Arrays on Silicon: Twin-Free down to the First Bilayer. *Nano Lett.* **2013**, *14*, 326-332.

(13) Gao, Q.; Saxena, D.; Wang, F.; Fu, L.; Mokkapati, S.; Guo, Y.; Li, L.; Wong-Leung, J.; Caroff, P.; Tan, H. H.; et al. Selective-Area Epitaxy of Pure Wurtzite InP Nanowires: High Quantum Efficiency and Room-Temperature Lasing. *Nano Lett.* **2014**, *14*, 5206-5211.

(14) Grosshans, F.; Van Assche, G.; Wenger, J.; Brouri, R.; Cerf, N. J.; Grangier, P. Quantum key distribution using gaussian-modulated coherent states. *Nature* **2003**, *421*, 238-241.
(15) Johnson, J. C.; Choi, H. J.; Knutsen, K. P.; Schaller, R. D.; Yang, P.; Saykally, R. J. Single gallium nitride nanowire lasers. *Nat. Mater.* **2002**, *1*, 106-110.
(16) Zimmler, M. A.; Bao, J.; Capasso, F.; Müller, S.; Ronning, C. Laser action in nanowires: Observation of the transition from amplified spontaneous emission to laser oscillation. *Appl. Phys. Lett.* **2008,** *93*, 051101-051103.
(17) Xiao, Y.; Meng, C.; Wang, P.; Ye, Y.; Yu, H.; Wang, S.; Gu, F.; Dai, L.; Tong, L. Single-nanowire single-mode laser. *Nano Lett.* **2011**, *11*, 1122-1126.
(18) Chin, A. H.; Vaddiraju, S.; Maslov, A. V.; Ning, C. Z.; Sunkara, M. K.; Meyyappan, M. Near-infrared semiconductor subwavelength-wire lasers. *Appl. Phys. Lett.* **2006**, *88*, 163115-163117.
(19) Chen, R.; Tran, T.-T. D.; Ng, K. W.; Ko, W. S.; Chuang, L. C.; Sedgwick, F. G.; Chang-Hasnain, C. Nanolasers grown on silicon. *Nat. Photon.* **2011**, *5*, 170-175.
(20) Lu, F.; Tran, T.-T. D.; Ko, W. S.; Ng, K. W.; Chen, R.; Chang-Hasnain, C. Nanolasers grown on silicon-based MOSFETs. *Opt. Exp.* **2012**, *20*, 12171-12176.
(21) Mayer, B.; Janker, L.; Rudolph, D.; Loitsch, B.; Kostenbader, T.; Abstreiter, G.; Koblmüller, G.; Finley, J. J. Continuous wave lasing from individual GaAs-AlGaAs core-shell nanowires. *Appl. Phys. Lett.* **2016,** *108*, 071107-071111.
(22) Burgess, T.; Saxena, D.; Mokkapati, S.; Li, Z.; Hall, C. R.; Davis, J. A.; Wang, Y.; Smith, L. M.; Fu, L.; Caroff, P.; et al. Doping-enhanced radiative efficiency enables lasing in unpassivated GaAs nanowires. *Nat. Commun.* **2016,** *7*, 11927-11933.
(23) Reimer, M. E.; Bulgarini, G.; Akopian, N.; Hocevar, M.; Bavinck, M. B.; Verheijen, M. A.; Bakkers, E.; Kouwenhoven, L. P.; Zwiller, V. Bright single-photon sources in bottom-up tailored nanowires. *Nat. Commun.* **2012,** *3*, 737-742.
(24) Qian, F.; Li, Y.; Gradecak, S.; Park, H. G.; Dong, Y.; Ding, Y.; Wang, Z. L.; Lieber, C. M. Multi-quantum-well nanowire heterostructures for wavelength-controlled lasers. *Nat. Mater.* **2008**, *7*, 701-706.
(25) Zhang, G.; Tateno, K.; Sanada, H.; Tawara, T.; Gotoh, H.; Nakano, H. Synthesis of GaAs nanowires with very small diameters and their optical properties with the radial quantum-confinement effect. *Appl. Phys. Lett.* **2009,** *95*, 123104-123106.
(26) Qian, F.; Gradečak, S.; Li, Y.; Wen, C.-Y.; Lieber, C. M. Core/Multishell Nanowire Heterostructures as Multicolor, High-Efficiency Light-Emitting Diodes. *Nano Lett.* **2005**, *5*, 2287-2291.
(27) Dimakis, E.; Jahn, U.; Ramsteiner, M.; Tahraoui, A.; Grandal, J.; Kong, X.; Marquardt, O.; Trampert, A.; Riechert, H.; Geelhaar, L. Coaxial multishell (In,Ga)As/GaAs nanowires for near-infrared emission on Si substrates. *Nano Lett.* **2014**, *14*, 2604-2609.
(28) Stettner, T.; Zimmermann, P.; Loitsch, B.; Döblinger, M.; Regler, A.; Mayer, B.; Winnerl, J.; Matich, S.; Riedl, H.; Kaniber, M.; et al. Coaxial GaAs-AlGaAs core-multishell nanowire lasers with epitaxial gain control. *Appl. Phys. Lett.* **2016,** *108*, 011108-011112.
(29) Erhard, N.; Zenger, S.; Morkötter, S.; Rudolph, D.; Weiss, M.; Krenner, H. J.; Karl, H.; Abstreiter, G.; Finley, J. J.; Koblmüller, G.; et al. Ultrafast Photodetection in the Quantum Wells of Single AlGaAs/GaAs-Based Nanowires. *Nano Lett.* **2015**, *15*, 6869-6874.
(30) Yan, X.; Zhang, X.; Li, J.; Wu, Y.; Cui, J.; Ren, X. Fabrication and optical properties of GaAs/InGaAs/GaAs nanowire core-multishell quantum well heterostructures. *Nanoscale* **2015**, *7*, 1110-1115.
(31) Shi, T.; Jackson, H. E.; Smith, L. M.; Jiang, N.; Gao, Q.; Tan, H. H.; Jagadish, C.; Zheng, C.; Etheridge, J. Emergence of Localized States in Narrow GaAs/AlGaAs Nanowire Quantum Well Tubes. *Nano Lett.* **2015**, *15*, 1876-1882.
(32) Mohan, P.; Motohisa, J.; Fukui, T. Fabrication of InP / InAs / InP core-multishell heterostructure nanowires by selective area metalorganic vapor phase epitaxy. *Appl. Phys. Lett.* **2006**, *88*, 133105-133107.

(33) Kawaguchi, K.; Nakata, Y.; Ekawa, M.; Yamamoto, T.; Arakawa, Y. In *Radial InP/InAsP quantum wells with high arsenic compositions on wurtzite-InP nanowires in the 1.3-µm region*, Indium Phosphide and Related Materials (IPRM), 2012 International Conference on, 27-30 Aug. 2012, 2012; pp 257-260.

(34) Zheng, C.; Wong-Leung, J.; Gao, Q.; Tan, H. H.; Jagadish, C.; Etheridge, J. Polarity-Driven 3-Fold Symmetry of GaAs/AlGaAs Core Multishell Nanowires. *Nano Lett.* **2013**, *13*, 3742-3748.

(35) Heiss, M.; Fontana, Y.; Gustafsson, A.; Wüst, G.; Magen, C.; O'Regan, D. D.; Luo, J. W.; Ketterer, B.; Conesa-Boj, S.; Kuhlmann, A. V.; et al. Self-assembled quantum dots in a nanowire system for quantum photonics. *Nat. Mater.* **2013**, *12*, 439-444.

(36) Saxena, D.; Jiang, N.; Yuan, X.; Mokkapati, S.; Guo, Y.; Tan, H. H.; Jagadish, C. Design and Room-Temperature Operation of GaAs/AlGaAs Multiple Quantum Well Nanowire Lasers. *Nano Lett.* **2016**, *16*, 5080-5086.

(37) Joyce, H. J.; Gao, Q.; Tan, H. H.; Jagadish, C.; Kim, Y.; Zhang, X.; Guo, Y.; Zou, J. Twin-Free Uniform Epitaxial GaAs Nanowires Grown by a Two-Temperature Process. *Nano Lett.* **2007**, *7*, 921-926.

(38) Jiang, N.; Wong-Leung, J.; Joyce, H. J.; Gao, Q.; Tan, H. H.; Jagadish, C. Understanding the true shape of Au-catalyzed GaAs nanowires. *Nano Lett.* **2014**, *14*, 5865-5872.

(39) Yuan, X.; Caroff, P.; Wang, F.; Guo, Y.; Wang, Y.; Jackson, H. E.; Smith, L. M.; Tan, H. H.; Jagadish, C. Antimony Induced {112}A Faceted Triangular GaAs1−xSbx/InP Core/Shell Nanowires and Their Enhanced Optical Quality. *Adv. Funct. Mater.* **2015,** *25*, 5300-5308.

(40) Wang, F.; Gao, Q.; Peng, K.; Li, Z.; Li, Z.; Guo, Y.; Fu, L.; Smith, L. M.; Tan, H. H.; Jagadish, C. Spatially Resolved Doping Concentration and Nonradiative Lifetime Profiles in Single Si-Doped InP Nanowires Using Photoluminescence Mapping. *Nano Lett.* **2015**, *15*, 3017-3023.

(41) Sun, L.; Ren, M. L.; Liu, W.; Agarwal, R. Resolving parity and order of Fabry-Perot modes in semiconductor nanostructure waveguides and lasers: Young's interference experiment revisited. *Nano Lett.* **2014**, *14*, 6564-6571.

(42) Yuan, X.; Caroff, P.; Wong-Leung, J.; Tan, H. H.; Jagadish, C. Controlling the morphology, composition and crystal structure in gold-seeded GaAs1-xSbx nanowires. *Nanoscale* **2015**, *7*, 4995-5003.

(43) Wagner, R. S.; Ellis, W. C. VAPOR ‐ LIQUID ‐ SOLID MECHANISM OF SINGLE CRYSTAL GROWTH. *Appl. Phys. Lett.* **1964,** *4*, 89-90.

(44) Conesa-Boj, S.; Hauge, H. I. T.; Verheijen, M. A.; Assali, S.; Li, A.; Bakkers, E. P. A. M.; Fontcuberta i Morral, A. Cracking the Si Shell Growth in Hexagonal GaP-Si Core–Shell Nanowires. *Nano Lett.* **2015**, *15*, 2974-2979.

(45) Huh, J.; Yun, H.; Kim, D.-C.; Munshi, A. M.; Dheeraj, D. L.; Kauko, H.; van Helvoort, A. T. J.; Lee, S.; Fimland, B.-O.; Weman, H. Rectifying Single GaAsSb Nanowire Devices Based on Self-Induced Compositional Gradients. *Nano Lett.* **2015**, *15*, 3709-3715.

(46) Jiang, N.; Parkinson, P.; Gao, Q.; Breuer, S.; Tan, H. H.; Wong-Leung, J.; Jagadish, C. Long minority carrier lifetime in Au-catalyzed GaAs/AlxGa1−xAs core-shell nanowires. *Appl. Phys. Lett.* **2012,** *101*, 023111-023114.

(47) Jiang, N.; Gao, Q.; Parkinson, P.; Wong-Leung, J.; Mokkapati, S.; Breuer, S.; Tan, H. H.; Zheng, C. L.; Etheridge, J.; Jagadish, C. Enhanced Minority Carrier Lifetimes in GaAs/AlGaAs Core–Shell Nanowires through Shell Growth Optimization. *Nano Lett.* **2013**, *13*, 5135-5140.

(48) Li, Z.; Yuan, X.; Fu, L.; Peng, K.; Wang, F.; Fu, X.; Caroff, P.; White, T.P.; Tan, H.H.; Jagadish, C. Room temperature GaAsSb single nanowire infrared photodetectors. *Nanotech.* **2015,** *26*, 445202-445209.

(49) Tchernycheva, M.; Lavenus, P.; Zhang, H.; Babichev, A. V.; Jacopin, G.; Shahmohammadi, M.; Julien, F. H.; Ciechonski, R.; Vescovi, G.; Kryliouk, O. InGaN/GaN Core–Shell Single Nanowire Light Emitting Diodes with Graphene-Based P-Contact. *Nano Lett.* **2014**, *14*, 2456-2465.

(50) Kuykendall, T.; Ulrich, P.; Aloni, S.; Yang, P. Complete composition tunability of InGaN nanowires using a combinatorial approach. *Nat. Mater.* **2007**, *6*, 951-956.

(51) Duan, X.; Huang, Y.; Agarwal, R.; Lieber, C. M. Single-nanowire electrically driven lasers. *Nature* **2003**, *421*, 241-245.
(52) Theeten, J. B.; Aspnes, D. E.; Chang, R. P. H. A new resonant ellipsometric technique for characterizing the interface between GaAs and its plasma ‐ grown oxide. *J. Appl. Phys.* **1978,** *49*, 6097-6102.
(53) Ferrini, R.; Patrini, M.; Franchi, S. Optical functions from 0.02 to 6 eV of AlxGa1−xSb/GaSb epitaxial layers. *J. Appl. Phys.* **1998,** *84*, 4517-4524.
(54) Palik, E. D., *Handbook of Optical Constants of Solids*. Academic Press: 2012; Vol. 2, p 1096.
(55) Saxena, D.; Wang, F.; Gao, Q.; Mokkapati, S.; Tan, H. H.; Jagadish, C. Mode Profiling of Semiconductor Nanowire Lasers. *Nano Lett.* **2015**, *15*, 5342-5348.
(56) Mokkapati, S.; Saxena, D.; Jiang, N.; Parkinson, P.; Wong-Leung, J.; Gao, Q.; Tan, H. H.; Jagadish, C. Polarization Tunable, Multicolor Emission from Core–Shell Photonic III–V Semiconductor Nanowires. *Nano Lett.* **2012**, *12*, 6428-6431.

## TOC Graphic